A Permanent Magnet Linear Motor for Micro Robots

Haiwei Lu, Jianguo Zhu, and Youguang Guo
CEMPE, Faculty of Engineering, University of Technology, Sydney
Sydney, Australia
haiwei@eng.uts.edu.au, joe@eng.uts.edu.au, youguang@eng.uts.edu.au

***Abstract*—Linear micro motors play a key role in micro robotic systems. They can greatly simplify the drive mechanisms and this is crucial for micro systems. By using permanent magnets, much higher force-to-volume ratios can be acquired than using electromagnets and better drive performance can be obtained. This paper describes the development of a tubular permanent magnet linear motor for the actuation of micro robots. Important design criteria are established by analytical method and numerical method is applied to obtain detailed characteristics of the micro motor. The performances of the micro motor are analyzed and predicted by the finite element analysis and dynamic modeling. The derived motor model is implemented in SIMULINK and is capable of being extending to complex robotic applications. The simulation of the motor operation shows that the dynamic performance is quite satisfactory.**

Keywords-linear motor; tubular; permanent magnet; micro robots

I. INTRODUCTION

Linear micro motors play a key role in micro robotic systems. Compared to those pneumatic or rotary-motor based drives, linear motors show significant advantages in terms of efficiency, thrust control, position accuracy, and system volume [1]. Particularly, linear motor can greatly simplify the drive mechanisms, and this is crucial for micro systems. By using permanent magnets (PMs) in the linear motors, much higher force-to-volume ratios and hence better drive performance than using electromagnets can be obtained.

The development of a tubular linear interior permanent magnet (TLIPM) motor for the actuation of micro robots is presented in this paper. Important design criteria are established by analytical method and numerical method is applied to obtain detailed characteristics of the micro motor. The performances of the micro motor are analyzed and predicted by the finite element (FE) analysis and dynamic modeling. The derived motor model is implemented in SIMULINK and can be extended to the robotic applications with more complex mechanical structure.

II. MICRO LINEAR MOTOR DESIGN

A. Linear Motor Structure

Fig.1 shows the basic configuration of the proposed TLIPM micro motor. The designed external radius R_e of the motor is around 3.5 mm. Three phase windings are mounted inside the stator core as shown in the figure. Due to the small external diameter, the slotless structure is chosen for simplicity in construction and better performance. The three-phase windings are arranged as *A-C-B-A-C-B-A-C-B* along the axial direction with the same pitch and each phase winding contains four ring-type coils connected in series. The material of the PMs used in the micro motor is Nd-Fe-B, and the material for the stator core is Glassy Metal, an amorphous soft magnetic ribbon material, which features high magnetic permeability and extremely low core loss. The armature shaft supporting the magnets and pole-pieces is made by non-ferromagnetic material (i.e. stainless steel) for some advantages such as reduction of the effective air gap between the stator and the armature, the volume of the PM material and the moving mass [2].

In order to determine the appropriate thickness of the PMs

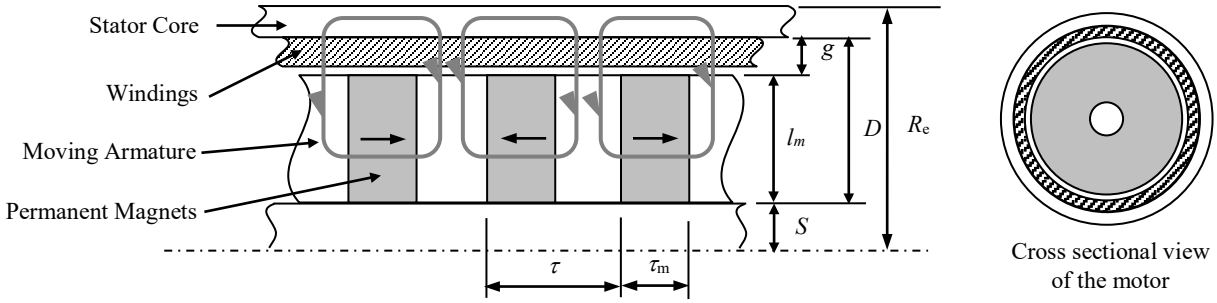

Figure 1. Configuration of the slotless TLIPM micro motor

and the diameter of the moving armature, an analytical analysis of magnetic field is firstly performed. Under the assumption of infinite magnetic permeability of the magnetic core and negligible leakage flux, by solving the magnetic circuit shown in the figure, the magnetic flux per pole pair ϕ_g can be worked out as:

$$\phi_g = \frac{\mu_0 \pi H_c \tau_m}{4g/[(2l_m + 2S + g)(\tau - \tau_m)] + \tau_m/[l_m(l_m + 2S)]} \quad (1)$$

where

H_c: the coercive force of the PM material;
τ: pole pitch of the armature;
τ_m: the width of the PM material;
l_m: radial depth of the PM material;
g: the gap between the stator and armature;
S: radius of the non-ferromagnetic shaft.

From (1), when keeping the volume of the motor and number of poles unchanged, say, taking l_m, g and τ as constants, the flux as well as the flux density in the air gap will vary with respect to the width of the PMs τ_m, as shown in Fig.2. It is seen that there exists a maximum flux at a certain width of PMs. By applying $d\phi_g/d\tau_m=0$, it can be found that the magnetic flux per pole pair will be maximum when $\tau_m=\tau/2$.

The electromagnetic force produced in the stator windings can be worked out by $F=BIL$. Based on the flux derived in (1) and applying $\tau_m=\tau/2$, the electromagnetic force per pole can be expressed as:

$$F_{em} = \mu_0 \pi H_c J_s k_f \frac{\tau^2 l_m (D - l_m)(2S + l_m)(D + 2S + l_m)}{16 l_m (D - l_m)(2S + l_m) + \tau^2 (D + 2S + l_m)} \quad (2)$$

where J_s is the current density of the stator windings, k_f the fill factor of the windings, and D the gap between the stator core and the shaft, as shown in Fig.1.

When the volume of the motor is limited, the gap D between the stator core and shaft is fixed. As a result, the produced electromagnetic force F_{em} is a function of l_m. It is noticed that there also exists an optimal value of l_m which makes the force reach its maximum value at the specified pole pitch and motor radius, and it can be found by solving $dF_{em}/dl_m=0$ from (2). For the designed dimensions of the motor, the variation of the force per pole with l_m is computed and is illustrated in Fig.3 in terms of the ratio of l_m/D. It can be found that the optimal ratio of l_m/D is 0.778 and the maximum force per pole is about 4.6 mN when the current density J_s is set to 6 A/mm^2 according to the thermal limit of the windings.

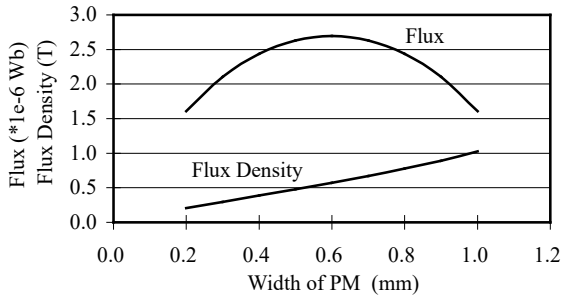

Figure 2. Flux and flux density in air gap vs. width of PM

The numerical method is applied to compare with the above analytical results. By a 2D FE analysis, the flux density in the air gap is analyzed and therefore the produced electromagnetic forces on the stator windings can be calculated. The electromagnetic force is calculated at different l_m/D ratios as shown in Fig.4 and the maximum force occurs near l_m/D=0.78. It can be seen that the numerical results agree well with the analytical results.

B. Flux Density and Magnetic Force

Since the moving armature of the micro motor is deliberately designed shorter than the stator so that it can move back and forth within the range of the stator windings, the distribution of the resultant flux density in the air gap varies with the position of the armature. Consequently, the produced electromagnetic force is also a function of the position of the armature. A 2D FE model is established to analyze the magnetic field in the TLIPM. Fig.5 shows the magnetic force line distribution when the armature is in the middle of the motor and Fig.6 shows the flux density distribution in the phase A windings with different armature positions.

Based on the analysis of the distribution of flux density in the air gap at different armature positions, the produced

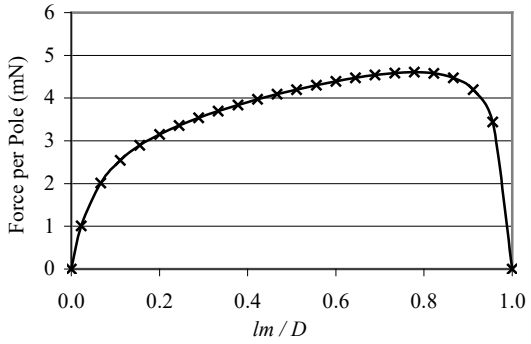

Figure 3. Electromagnetic force vs. the ratio of l_m/D

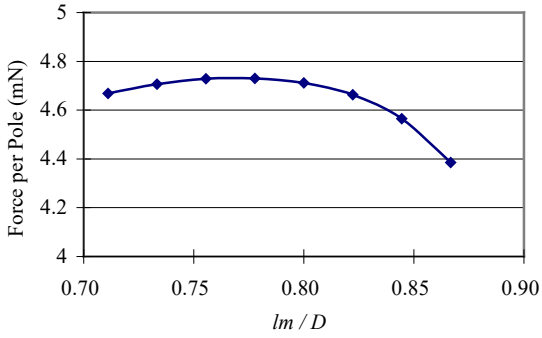

Figure 4. Electromagnetic force vs. the ratio of l_m/D by FE analysis

magnetic force can be predicted. The results can provide an optimal current commutation scheme for the motor controller. Fig.7 shows the motor force at different armature positions when also applying a current density of 6 A/mm^2 and a suitable current switching sequence under brushless DC drive scheme.

C. *Stator Winding Inductances*

The stator winding inductance is one of the most important parameters for the motor modeling, performance simulation and controller design. In this paper, the energy method is applied for the inductance computation. However, due to the non-linear properties of the magnetic core, it is difficult to use 2D FE model to work out the stored magnetic energy in such a tubular structure. Thus, a 3D FE model is applied and during the analysis, the saturation effect is considered to improve the accuracy of calculation.

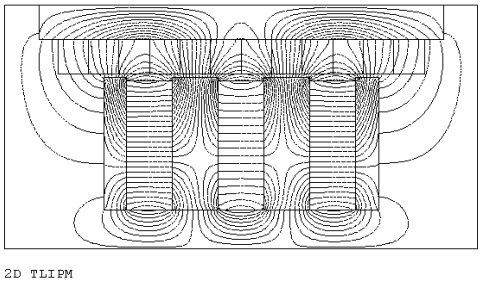

Figure 5. 2D flux distribution in the TLIPM

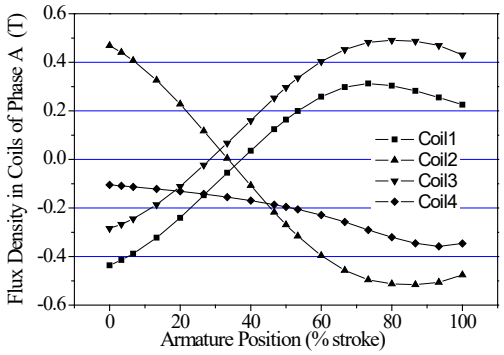

Figure 6. Flux density under phase A

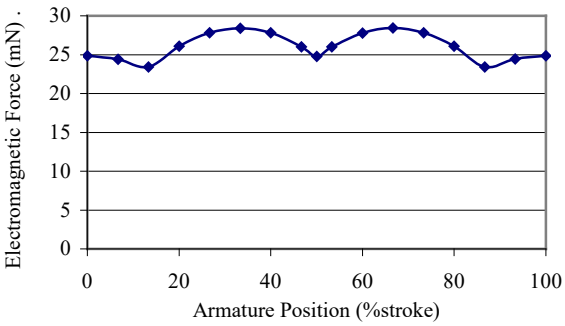

Figure 7. Motor force vs. armature positions

Because of the non-linear properties of the Glassy Metal, it is necessary to find out the operation point set by the PMs before the magnetic energy produced by the stator current can be correctly obtained. Fig.8 shows the flux density produced only by the PMs via a 3D non-linear FE model. Based on the results, the magnetic flux density in each part of the magnetic core of the motor can be obtained and the related magnetic permeability can be found. Table I lists the relative permeability in different magnetic core regions.

It is shown in Table I that the armature core, especially the pole-pieces in the middle of the armature, is saturated. Taking the results as the operation point, the magnetic energy generated by the stator winding current is calculated by "switching off" the PMs, and the inductances of the windings can then be obtained by the energy method. Table II shows the computational results at two different armature positions.

It is noted that the mutual inductance between phases A and B, L_{ab}, is much smaller than the other two mutual inductances. This is due to the unsymmetrical distribution of the phase windings, which makes the coupling effect between phase A and B less than that of the others.

III. DYNAMIC MODEL OF TLIPM

A comprehensive dynamic model is essential for analyzing the performance of an electric machine. The previous electromagnetic field analysis and parameter identification of the TLIPM provide the basic information of the motor for establishing a system model.

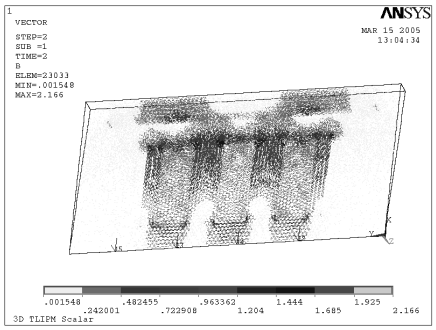

Figure 8. 3D FE model of TLIPM with flux density distribution

TABLE I RELATIVE PERMEABILITY IN DIFFERENT MOTOR PARTS

Armature core Upper	Armature core 2nd layer	Armature core 3rd layer	Armature core Bottom	Stator core
258	121	121	275	478400

TABLE II STATOR WINDING SELF AND MUTUAL INDUCTANCES (UNIT: μH)

Position	L_a	L_b	L_c	L_{ab}	L_{bc}	L_{ac}
0% stroke	61.3	61.2	62.2	8.67	32.1	31.9
50% stroke	61.4	61.4	61.7	13.1	30.0	30.0

A. Flux Linkage and Back EMF

In order to analyze the flux linkage of the proposed TLIPM, an enclosed cylindrical coil pair is studied in advance. Fig.9(a) shows the schematic structure of such an enclosed cylindrical coil pair. When the coil pair is put into a uniform radial magnetic field, as shown in Fig.9(b), the flux linkage of the coil can be obtained as:

$$\lambda_m = N\int_S B_r(z)ds = 2\pi rN\int_{z_0-c_w/2}^{z_0+c_w/2} B_r(z)dz \tag{3}$$

where:

N: number of turns of the coil;
r: mean radius of the coil;
$B_r(z)$: the radial component of the flux density within the coil;
S: the cylindrical surface area of the coil;
z_0: the center position of the coil pair, as shown in Fig.9(a);
c_w: the span of the coil pair.

If there is a relative movement between the coil and external magnetic field, a back *EMF* will be generated in the coil and can be obtained by Faraday's Law as

$$e = -2\pi rN[B_r(z_0 + c_w/2) - B_r(z_0 - c_w/2)]v_z \tag{4}$$

where v_z is the relative velocity between the coil and the magnetic field in z direction.

For the TLIPM shown in Fig.1, the total flux linkage of each phase can be expressed as:

$$\lambda_i = \lambda_{ii} + \lambda_{ij} + \lambda_{ik} + \lambda_{im},\ i,j,k \in (a,b,c),\ i \neq j \neq k \tag{5}$$

where λ_{ii}, λ_{ij} and λ_{ik} are the flux linkages of phase i that produced by the currents in phase i, j and k, respectively, and λ_{im} *is* the magnetizing flux linkage produced by the PMs on the armature. Since the flux linkage can be expressed as $\lambda=Li$, (5) can be further written as:

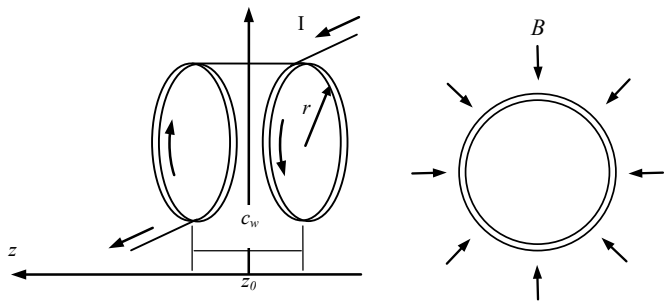

(a) (b)

Figure 9. An enclosed cylindrical coil pair

$$\lambda_i = L_{ii}i_i + L_{ij}i_j + L_{ik}i_k + \lambda_{im} \tag{6}$$

where L_{ii} is the self-inductance of each phase, L_{ij}, L_{ik} are the mutual inductances between phases, and $L_{ab}=L_{ba}$, $L_{bc}=L_{cb}$, and $L_{ac}=L_{ca}$.

The above magnetizing flux linkage of each phase can be worked out based on the previous analysis of the flux linkage of an enclosed cylindrical coil pair. Since each phase winding of the TLIPM contains two enclosed cylindrical coil pairs connected in series, the magnetizing flux linkages of each cylindrical coil pair in the three-phase-windings can be found as:

$$\lambda_{imn} = 2\pi rN\int_{z_{i0n}-c_w/2}^{z_{i0n}+c_w/2} B_r(z)dz,\ i \in (a,b,c),\ n = 1,2 \tag{7}$$

where z_{i0n} is the center position of each coil pair in the phase windings. As a result, the total magnetizing flux linkage of each phase is the sum of that of each coil pair:

$$\lambda_{im} = \sum_{n=1}^{2}\lambda_{imn},\ i \in (a,b,c) \tag{8}$$

B. Electric Circuit Equations

The electrical circuit equation of each phase can be written as:

$$v_a = R_a i_a + d\lambda_a/dt \tag{9}$$

$$v_b = R_b i_b + d\lambda_b/dt \tag{10}$$

$$v_c = R_c i_c + d\lambda_c/dt \tag{11}$$

Based on the analysis of flux linkage in phase windings, $d\lambda_a/dt$, as an example, can be expressed as:

$$\begin{aligned}\frac{d\lambda_a}{dt} &= L_{aa}\frac{di_a}{dt} + i_a\frac{dL_{aa}}{dt} + L_{ab}\frac{di_b}{dt} + i_b\frac{dL_{ab}}{dt} \\ &+ L_{ac}\frac{di_c}{dt} + i_c\frac{dL_{ac}}{dt} + e_{am}\end{aligned} \tag{12}$$

where $e_{am}=d\lambda_{am}/dt$ is the back *EMF* produced by the magnetizing flux of PMs.

If the saliencies and saturation effect are not considered, the inductances are constants and (12) can be simplified as:

$$\frac{d\lambda_a}{dt} = L_{aa}\frac{di_a}{dt} + L_{ab}\frac{di_b}{dt} + L_{ac}\frac{di_c}{dt} + e_{am} \tag{13}$$

Then the circuit equation of phase A can be rewritten as:

$$v_a = R_a i_a + L_{aa}\frac{di_a}{dt} + L_{ab}\frac{di_b}{dt} + L_{ac}\frac{di_c}{dt} + e_{am} \tag{14}$$

and the back *EMF* can be obtained based on (4):

$$\begin{aligned} e_{am} &= 2\pi rN[B_r(z_{a01} + {}^{c_w}\!/_2) + B_r(z_{a02} + {}^{c_w}\!/_2) \\ &\quad - B_r(z_{a01} - {}^{c_w}\!/_2) - B_r(z_{a02} - {}^{c_w}\!/_2)]v_z \end{aligned} \tag{15}$$

Similarly, the relationship in phase B and C can be obtained as:

$$v_b = R_b i_b + L_{ba}\frac{di_a}{dt} + L_{bb}\frac{di_b}{dt} + L_{bc}\frac{di_c}{dt} + e_{bm} \tag{16}$$

$$v_c = R_c i_c + L_{ca}\frac{di_a}{dt} + L_{cb}\frac{di_b}{dt} + L_{cc}\frac{di_c}{dt} + e_{cm} \tag{17}$$

$$\begin{aligned} e_{bm} &= 2\pi rN[B_r(z_{b01} + {}^{c_w}\!/_2) + B_r(z_{b02} + {}^{c_w}\!/_2) \\ &\quad - B_r(z_{b01} - {}^{c_w}\!/_2) - B_r(z_{b02} - {}^{c_w}\!/_2)]v_z \end{aligned} \tag{18}$$

$$\begin{aligned} e_{cm} &= 2\pi rN[B_r(z_{c01} + {}^{c_w}\!/_2) + B_r(z_{c02} + {}^{c_w}\!/_2) \\ &\quad - B_r(z_{c01} - {}^{c_w}\!/_2) - B_r(z_{c02} - {}^{c_w}\!/_2)]v_z \end{aligned} \tag{19}$$

C. *Electromagnetic Force of the Motor*

The electromagnetic force of the motor can be worked out by derivative of the corresponding system co-energy with respect to the displacement, i.e. $F_{em}=\partial W_f'/\partial z$. According to the flux linkage in the previous flux linkage model, the contributed co-energy of each phase can be found as:

$$W_a' = \int_0^{i_a} (L_{aa}i_a + L_{ab}i_b + L_{ac}i_c + \lambda_{am})di_a \tag{20}$$

$$W_b' = \int_0^{i_b} (L_{ba}i_a + L_{bb}i_b + L_{bc}i_c + \lambda_{bm})di_b \tag{21}$$

$$W_c' = \int_0^{i_c} (L_{ca}i_a + L_{cb}i_b + L_{cc}i_c + \lambda_{cm})di_c \tag{22}$$

If the saturation effect caused by the stator currents is not considered, the inductances can be considered as constants, and (20) to (22) can be expressed as:

$$W_a' = \tfrac{1}{2}L_{aa}i_a^2 + L_{ab}i_b i_a + L_{ac}i_c i_a + \lambda_{am}i_a \tag{23}$$

$$W_b' = L_{ba}i_a i_b + \tfrac{1}{2}L_{bb}i_b^2 + L_{bc}i_c i_b + \lambda_{bm}i_b \tag{24}$$

$$W_c' = L_{ca}i_a i_c + L_{cb}i_b i_c + \tfrac{1}{2}L_{cc}i_c^2 + \lambda_{cm}i_c \tag{25}$$

The total corresponding co-energy of the motor is:

$$W_f' = W_a' + W_b' + W_c' \tag{26}$$

and the electromagnetic force is then found as:

$$F_{em} = \frac{\partial \lambda_{am}}{\partial z}i_a + \frac{\partial \lambda_{bm}}{\partial z}i_b + \frac{\partial \lambda_{cm}}{\partial z}i_c \tag{27}$$

$\partial\lambda_{am}/\partial z$, $\partial\lambda_{bm}/\partial z$ and $\partial\lambda_{cm}/\partial z$ in (27) can be solved by the same method used for analyzing the back *EMF*. Thus, F_{em} can be further obtained as:

$$\begin{aligned} F_{emm} &= 2\pi rN[B_r(z_{a01} + {}^{c_w}\!/_2) + B_r(z_{a02} + {}^{c_w}\!/_2) \\ &\quad - B_r(z_{a01} - {}^{c_w}\!/_2) - B_r(z_{a02} - {}^{c_w}\!/_2)]i_a \\ &\quad + 2\pi rN[B_r(z_{b01} + {}^{c_w}\!/_2) + B_r(z_{b02} + {}^{c_w}\!/_2) \\ &\quad - B_r(z_{b01} - {}^{c_w}\!/_2) - B_r(z_{b02} - {}^{c_w}\!/_2)]i_b \\ &\quad + 2\pi rN[B_r(z_{c01}' - {}^{c_w}\!/_2) + B_r(z_{c02}' - {}^{c_w}\!/_2) \\ &\quad - B_r(z_{c01}' + {}^{c_w}\!/_2) - B_r(z_{c02}' + {}^{c_w}\!/_2)]i_c \end{aligned} \tag{28}$$

D. *State Equations of the Motor*

Based on the above analysis, combined with the kinetic equation, one can form the state equations of the designed TLIPM. In order to make it clear, these equations are rewritten in the matrix format as:

$$\begin{bmatrix} di_a/dt \\ di_b/dt \\ di_c/dt \end{bmatrix} = \begin{bmatrix} L_{aa} & L_{ab} & L_{ac} \\ L_{ba} & L_{bb} & L_{bc} \\ L_{ca} & L_{cb} & L_{cc} \end{bmatrix}^{-1} \begin{bmatrix} v_a - e_{am} - R_a i_a \\ v_b - e_{bm} - R_b i_b \\ v_c - e_{cm} - R_c i_c \end{bmatrix}$$
$$dv_z/dt = F_{em}/m_a \tag{29}$$

where m_a is the mass of the armature. The back *EMF* and electromagnetic force can be found using (15), (18), (19) and (28). The radial component of flux density within each phase coil, $B_r(z)$, which is required for finding the back *EMF* and electromagnetic force , is obtained via FE analysis.

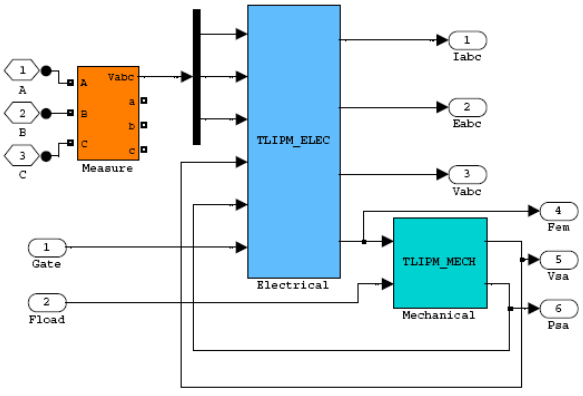

Figure 10 Simulink model of the TLIPM

IV. STUDY OF MOTOR PERFORMACE

A. *Simulink Model of the TLIPM*

A SIMULINK model is established according to the dynamic model derived in section III. Fig.10 shows the block diagram of the model implemented in SIMULINK environment. The model contains two blocks: the electrical block and the mechanical block. Both blocks are implemented via the SIMULINK S-function block by utilizing the state equations of the motor.

The electrical block calculates the phase currents, back *EMFs* and electromagnetic force of the motor based on its input phase voltages. The input phase voltages can be either balanced sinusoidal waveforms or switched waveforms such as PWM voltages. The electromagnetic force and the load force are input to the mechanical block to find out the velocity and displacement of the moving parts of the motor. The mechanical block can be further reconfigured according to the different kinetic properties when the motor is applied in a robotic system, and thus the corresponding kinetic performances can be found correctly.

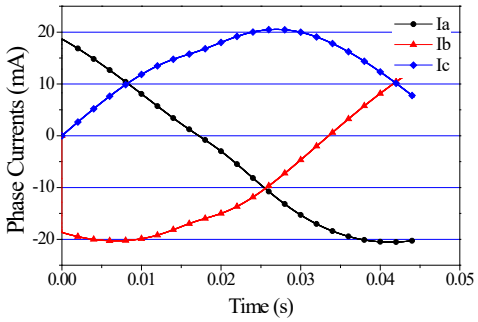

(a) Phase Currents

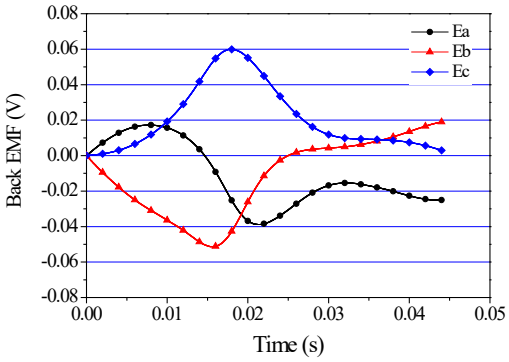

(b) Back EMF

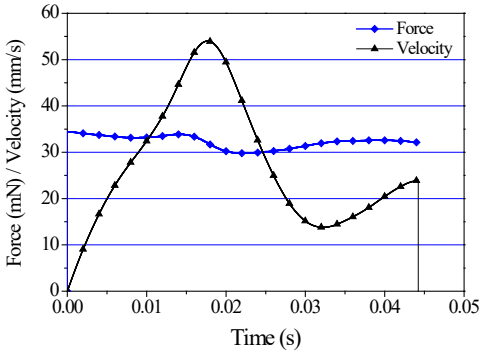

(c) Force and Velocity

Figure 11. Simulation results of the TLIPM performance under 3-ph excitation

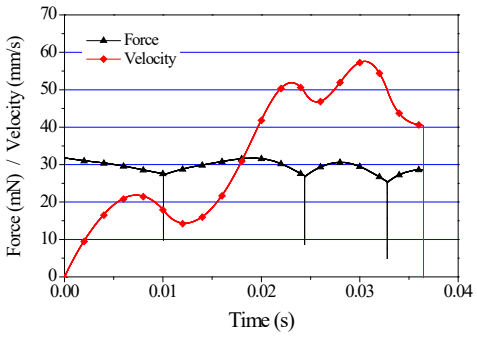

Figure 12 Simulation results of the TLIPM performance with BLDC drive

B. *Simulation of Motor Performance*

The dynamic performances of the TLIPM are studied based on the established SIMULINK model. Because the proposed linear motor is designed for the application of micro robotics, the control strategy should be as simple as possible to avoid complex hardware requirement of the control system.

Firstly, the motor is driven by a balanced three phase voltages without any closed-loop control. The initial phase angle of the input voltage is selected according to the armature position so that an optimal torque can be generated. The amplitude of the input voltage is selected according to the allowable *rms* current density discussed in Section II. The armature will stop when it reaches its full stroke, which is about 1.2 mm. Fig.11 shows the phase currents, back *EMF*, force and armature speed when the load force is set to its maximum allowable value. It is seen that there is a significant fluctuation in speed due to the open-loop strategy.

A brushless DC drive scheme with position sensor is also tried on this machine and the force and armature speed are shown in Fig.12. The commutation points for the brushless DC drive are obtained via force analysis explained in Section II-C. It is shown that the maximum force is smaller than that in 3-phase excitation but the speed is smoother. A suitable sensorless control scheme for this micro machine is under development.

V. CONCLUSION

A PM micro linear motor has been developed for linear motion micro robotic systems. Important design criteria are established by the analytical study of the flux and electromagnetic force of the motor. Numerical solutions of the magnetic field give detailed characteristics of the micro motor and the parameters are then derived. The dynamic model of the proposed motor is derived by using the results obtained from the field analysis, and is implemented within SIMULINK environment. Dynamic simulation is made under 3-phase

excitation and brushless DC drive scheme. The results show satisfactory performances of the proposed motor.

REFERENCES

[1] N. Bianchi, S. Bolognani, and F. Tonel, "Design consideration for a tubular linear PM servo motor," EPE Journal, vol. 11, no. 3, Aug. 2001, pp. 41-47.

[2] J. Wang, D. Howe, and G. W. Jewell, "Analysis and design optimization of an improved axially magnetized tubular permanent-magnet machine," IEEE Trans. Energy Conversion, vol. 19, no. 2, June 2004, pp. 289-295.

[3] B. Lequesne, "Permanent magnet linear motors for short strokes," IEEE Trans. Ind. Applicat., vol. 32, no. 1, Jan./Feb. 1996, pp. 161-168.